Draft version February 11, 2018
Typeset using LaTeX **twocolumn** style in AASTeX61

THERMONUCLEAR REACTION RATES FOR TRITIUM + DEUTERIUM FUSION USING BAYESIAN METHODS

Rafael S. de Souza,[1] Christian Iliadis,[1] S. Reece Boston,[1] and Alain Coc[2]

[1] *Department of Physics & Astronomy, University of North Carolina at Chapel Hill, NC 27599-3255, USA*
[2] *Centre de Sciences Nucléaires et de Sciences de la Matière, Univ. Paris-Sud, CNRS/IN2P3, Université Paris-Saclay, Bâtiment, 104, F-91405 Orsay Campus, France*

(Received February 11, 2018)

Submitted to ApJ

ABSTRACT

xxx.

Keywords: bayesian

Corresponding author: Christian Iliadis
iliadis@unc.edu

1. INTRODUCTION

The cross section of the ^{3}H(d,n)α reaction has a large Q-value of 17.6 MeV, and a large cross section that peaks at a value of $\approx$ 5 barn near a deuteron (or triton) bombarding energy of 105 keV (or 164 keV). For these reasons, the ^{3}H(d,n)α reaction will most likely fuel the first magnetic and inertial confinement fusion reactors for commercial energy production. The reactors are expected to operate in the thermal energy range of kT= 1 $-$ 30 keV, corresponding to temperatures of T= 12 $-$ 350 MK. These values translate to kinetic energies between 4 keV and 120 keV in the ^{3}H + d center-of-mass system, which can be compared with a height of $\approx$280 keV for the Coulomb barrier. The ^{3}H(d,n)α reaction also occurs during big bang nucleosynthesis, at temperatures between 0.5 GK and 1.0 MK, corresponding to center-of-mass energies in the range of 13 $-$ 252 keV.

The low-energy cross section is dominated by a ^{3}H + d s-wave resonance with a spin-parity of $J^\pi = 3/2^+$, corresponding to the second excited level near E_x = 16.7 MeV excitation energy in the ^{5}He compound nucleus (Tilley et al. 2002). The compound level decays via emission of d-wave neutrons. This level has mainly a ^{3}H + d structure, corresponding to a large deuteron spectroscopic factor (Barker 1997), while shell model calculations predict a relatively small neutron spectrocopic factor (Barker & Woods 1985). At the same time, the neutron penetrability is much larger than the deuteron penetrability at these low energies, so that incidentally the partial widths, given by the product of spectroscopic factor and penetrability, for the deuteron and neutron channel (Γ_d, Γ_n) become similar in magnitude. Considering a simple Breit-Wigner expression, the cross section maximum is proportional to $\Gamma_d\Gamma_n/(\Gamma_d + \Gamma_n)^2$, which peaks for the condition $\Gamma_d \approx \Gamma_n$. Therefore, the near equality of the deuteron and neutron partial widths causes the large low-energy cross section of the ^{3}H(d,n)α reaction (Conner et al. 1952; Argo et al. 1952).

For the design of fusion reactors and for purposes of plasma diagnostics, it is important to know the ^{3}H(d,n)α thermonuclear rate with the greatest possible accuracy. Different strategies to analyze the data were adopted in the past. Fits of the available ^{3}H(d,n)α data using Breit-Wigner expressions were reported by Duane (1972) and Angulo et al. (1999), while a Padé expansion was used in Peres (1979). Single-level and multi-level R-matrix fits to ^{3}H(d,n)α data were discussed by Jarmie et al. (1984); Brown et al. (1987); Barker (1997); Descouvemont et al. (2004). A comprehensive R-matrix approach, which in addition to the ^{3}H(d,n)α data included elastic and inelastic cross sections of the ^{3}H + d and ^{4}He + n systems, incorporating 2664 data points and 117 free parameters, was presented by Hale, Brown & Jarmie (1987); Bosch & Hale (1992). An analysis of ^{3}H(d,n)α data using effective field theory, with only three fitting parameters, can be found in Brown & Hale (2014).

In the present work, we are mainly concerned with quantifying the uncertainties in the thermonuclear rates (or reactivities) of the ^{3}H(d,n)α reaction. All previous works employed traditional statistics in the data fitting. Here, we will discuss an analysis using Bayesian techniques. Such a study, for the analog ^{3}He(d,p)^{4}He reaction, has been published recently by de Souza et al. (2018). The Bayesian approach has major advantages, as discussed by Iliadis et al. (2016); Gómez Iñesta et al. (2017). In addition, all previous R-matrix analyses kept the channel radii constant during the fitting. In reality, these quantities are poorly constrained, and thus our limited knowledge will impact the uncertainies of the derived S-factors and thermonuclear rates.

In Section 2, we briefly present the S-factor data adopted in the present work. Section 3 summarizes the reaction formalism. Our Bayesian model for fitting the S-factor data is discussed in Section 4, including likelihoods, model parameters, and priors. In Section 6, we present Bayesian thermonuclear reaction rates. A summary and conclusions are given in Section 7. The appendix discusses in more detail the data we adopted in our analysis.

2. DATA SELECTION

Several previous works have indiscriminately used all of the available ^{3}H + d cross section data in the fitting. In the present work, we will only select those measurements for which we can separately estimate the statistical and systematic contributions to the total uncertainties. For a given experiment, statistical uncertainties fluctuate randomly from data point to data point, whereas systematic uncertainties are correlated from data point to data point, such that if one happened to know how to correct such an uncertainty for one data point, then one could calculate the correction at the other data points as well.

The ^{3}H(d,n)α low-energy cross section is a steep function of energy. For example, at 20 keV in the center of mass, a 0.1 keV change in energy causes a 2% change in cross section, while at 10 keV, a 0.1 keV change causes a 6% change in cross section. Therefore, the accurate knowledge of the incident beam energy becomes crucial for the data analysis. Experiments that employed thin targets will be less prone to systemic effects than those using thick targets. For example, consider the data measured by Argo et al. (1952), which were adopted at face value in previous thermonuclear rate determina-

tions. Argo et al. (1952) employed 1.5 mg/cm^2 thick aluminum entrance foils for their deuterium gas target. Under such conditions, tritons of 183 keV laboratory energy after passing the entrance foil would have lost 568 keV in the foil, giving rise to an overall beam straggling of ≈ 31 keV. In this case, it is difficult to correct the measured cross section for the beam energy loss. Compare this situation to the measurement by Jarmie et al. (1984), where the triton beam lost less than 200 eV energy while traversing a windowless deuterium gas target. A detailed discussion of all data sets that have been adopted or disregarded in the present analysis is given in the appendix.

All the data we have adopted are shown in Figure 1. They originated from the experiments by Arnold et al. (1953); Kobzev et al. (1966); Jarmie et al. (1984); Brown et al. (1987). Notice that the results of Brown et al. (1987) have been used at face value in previous thermonuclear rate determinations, although these authors did not determined any absolute cross sections. We will discuss in Section 5.2 how to implement such data in a consistent manner into the Bayesian model.

3. REACTION FORMALISM

Since we are mainly interested in the low-energy region, where the $3/2^+$ s-wave resonance dominates the cross section, we will follow Barker (1997) and describe the theoretical energy dependence of the cross section using a one-level, two-channel R-matrix approximation.

The integrated cross section of the ^{3}He(d,n)^{4}He reaction is given by

$$\sigma_{dn}(E) = \frac{\pi}{k^2}\frac{2J+1}{(2j_1+1)(2j_2+1)}\,|S_{dn}|^2 \qquad (1)$$

where k and E are the wave number and energy, respectively, in the ^{3}H + d center-of-mass system, $J = 3/2$ is the resonance spin, $j_1 = 1/2$ and $j_2 = 1$ are the ground-state spins of the triton and deuteron, respectively, and S_{dn} is a scattering matrix element. The corresponding astrophysical S-factor is defined by

$$S_{bare}(E) \equiv E e^{2\pi\eta}\sigma_{dn}(E) \qquad (2)$$

where η is the Sommerfeld parameter. The scattering matrix element can be expressed as (Lane & Thomas 1958)

$$|S_{dn}|^2 = \frac{\Gamma_d\Gamma_n}{(E_0+\Delta-E)^2+(\Gamma/2)^2} \qquad (3)$$

where E_0 denotes the level eigenenergy. The partial widths of the ^{3}H + d and ^{4}He + n channels (Γ_d, Γ_n), the total width (Γ), and total level shift (Δ), which are all energy dependent, are given by

$$\Gamma = \sum_c \Gamma_c = \Gamma_d + \Gamma_n\ , \quad \Gamma_c = 2\gamma_c^2 P_c \qquad (4)$$

$$\Delta = \sum_c \Delta_c = \Delta_d + \Delta_n\ , \quad \Delta_c = -\gamma_c^2(S_c - B_c) \qquad (5)$$

where γ_c^2 is the reduced width, and B_c is the boundary condition parameter. The energy-dependent quantities P_c and S_c denote the penetration factor and shift factor, respectively, for channel c (either d + ^{3}H or n + ^{4}He). They are computed numerically from the Coulomb wave functions, F_ℓ and G_ℓ, according to

$$P_c = \frac{ka_c}{F_\ell^2+G_\ell^2}\ , \quad S_c = \frac{ka_c(F_\ell F_\ell' + G_\ell G_\ell')}{F_\ell^2+G_\ell^2} \qquad (6)$$

The Coulomb wave functions and their derivatives are evaluated at the channel radius, a_c; ℓ denotes the orbital angular momentum for a given channel.

In some cases, the fit to the data can be improved by adding a distant level in the analysis, located at a fixed energy outside the range of interest. However, such "background poles" have no physical meaning. As will become apparent below, the single-level, two-channel approximation represents a satisfcatory model for the low-energy data of interest here.

Teichmann & Wigner (1952) showed that the reduced width, $\gamma_{\lambda c}^2$, of an eigenstate λ cannot exceed, on average, the single-particle limit, given by

$$\langle\gamma_{\lambda c}^2\rangle \lesssim \frac{3}{2}\frac{\hbar^2}{m_c a_c^2} \qquad (7)$$

where m_c is the reduced mass of the interacting pair of particles in channel c. In this original formulation, the inequality only holds for a reduced width that is averaged over many eigenstates λ. Using the actual strength of the residual interaction in nuclei, Dover, Mahaux & Weidenmüller (1969) found for an individual resonance in a nucleon channel a single-particle limit of

$$\gamma_{\lambda c}^2 \lesssim \frac{\hbar^2}{m_c a_c^2} \qquad (8)$$

The quantity $\gamma_{WL}^2 \equiv \hbar^2/(m_c a_c^2)$ is often referred to as the Wigner limit. Considering the various assumptions made in deriving the above expressions, the Wigner limit provides only an approximation for the maximum value of a reduced width.

We perform the S-factor fit to the data using the expression (Assenbaum, Langanke & Rolfs 1987; Engstler et al. 1988)

$$S(E) \approx S_{bare}(E) e^{\pi\eta(U_e/E)} \qquad (9)$$

where U_e is the energy-independent electron screening potential. The latter quantity, which has a positive

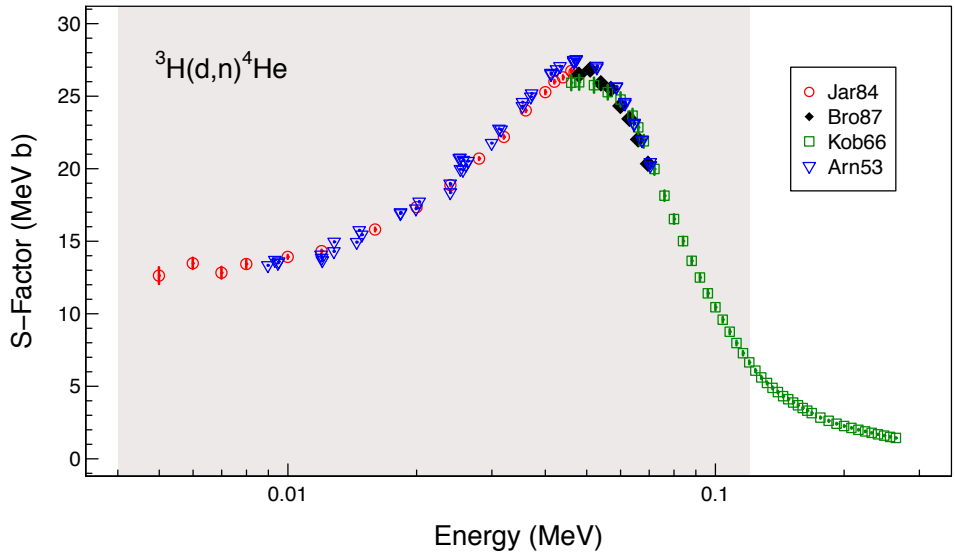

Figure 1. The data used in our analysis: (Red circles) Jarmie et al. (1984); (Blue triangles) Arnold et al. (1953); (Black diamonds) Brown et al. (1987); (Green squares) Kobzev et al. (1966). Absolute cross sections were not determined in Brown et al. (1987) and their data were normalized to those of Jarmie et al. (1984). Only statistical uncertainties are shown, but for many data points they are smaller than the symbol size. The shaded area marks the energy region important for fusion reactors. Details are given in the appendix.

value, depends on the identities of target and projectile, i.e., it differs for forward and inverse kinematics experiments.

R-matrix parameters and cross sections derived from data have a well-known dependence on the channel (or interaction) radius, which is usually expressed as

$$a_c = r_0 \left(A_1^{1/3} + A_2^{1/3} \right) \tag{10}$$

where A_i are the mass numbers of the two interacting nuclei, and r_0 is the radius parameter with a value usually chosen between 1.4 fm and 1.5 fm. This dependence arises from the truncation of the R-matrix to a restricted number of poles (i.e., a finite set of eigenenergies). The radius of a given channel has no rigorous physical meaning, except that the chosen values should exceed the sum of the radii of the colliding nuclei (see, e.g., Descouvemont & Baye (2010), and references therein). The channel radius dependence can likely be reduced by including more levels (including background poles) in the data analysis, but only at the cost of increasing the number of fitting parameters. In any case, it is important to include the effects of varying the channel radius in the data analysis. We will return to this issue in Section 5.

Another issue that needs investigating is the effect of the arbitrary choice of boundary condition parameter, B_c. It can be seen from Equations 3 and 5 that changing B_c will result in a corresponding change of the eigenenergy, E_0, to reproduce the measured location of the cross section maximum. In the one-level approximation, B_c should be chosen so that the eigenvalue E_0 lies within the width of the observed resonance (Lane & Thomas 1958). For a relatively narrow resonance, one can assume that the maximum of the scattering matrix element (Equation 3) occurs at an energy E_r, defined by $E_0 + \Delta(E_r) - E_r = 0$. In that case, the customary choice for the boundary condition parameter is $B_c = S_c(E_r)$. This choice results in $\Delta(E_r) = 0$, or $E_r = E_0$, and certainly fulfills this requirement. As will be discussed in Section 5, the situation is not so obvious in the case of the broad low-energy resonance in ^{3}H(d,n)^{4}He.

4. BAYESIAN MODELS

4.1. *General Aspects*

We analyze the S-factor data using Bayesian statistics and Markov chain Monte Carlo (MCMC) algorithms. For applications to nuclear astrophysics, the method has been discussed in Iliadis et al. (2016) and Gómez Iñesta et al. (2017). Bayes' theorem is given by (Jaynes & Bretthorst 2003)

$$p(\theta|y) = \frac{\mathcal{L}(y|\theta)\pi(\theta)}{\int \mathcal{L}(y|\theta)\pi(\theta)d\theta} \tag{11}$$

where the data are denoted by y and the complete set of model parameters is described by the vector θ. All of the factors entering in Equation 11 represent probability densities: $\mathcal{L}(y|\theta)$ is the likelihood, i.e., the probability that the data, y, were obtained assuming given values of the model parameters; $\pi(\theta)$ is called the prior, which represents our state of knowledge before seeing the data; the product of likelihood and prior defines the posterior,

$p(\theta|y)$, i.e., the probability of the values of a specific set of model parameters given the data; the denominator, called the evidence, is a normalization factor and is not important in our context. It can be seen from Equation 11 that the posterior represents an update in our state of prior knowledge about the model parameters once new data become available.

Of particular interest for the present work is the concept of a hierarchical Bayesian model (Hilbe, de Souza & Ishida 2017, and references therein). It allows us, in the data analysis, to take all relevant effects and processes into account that affect the measured data, which is frequently not possible with traditional statistics. Consider a simple example of a nuclear counting experiment. The true mean value of the decay rate cannot be observed directly and is only known to mother nature. The *actual* number of decays differs from the *true* mean value by a random amount, ϵ_{stoc}, because of the stochastic nature of a nuclear process. However, we cannot observe directly the actual number of decays because its value is perturbed by the measurement apparatus, first by systematic effects (which changes the actual value by an amount of ϵ_{syst}), and second by statistical effects (which gives rise to an additional change by ϵ_{stat}). The former affect all data points in a given set similarly, while the latter affect each data point differently. It is straightforward to construct the Bayesian model that incorporates all of these different layers of perturbations (ϵ_{stoc}, ϵ_{syst}, ϵ_{stat}). The overall goal is to estimate credible values for the true (but unknown) decay rate based on the measured data.

The random sampling of the posterior is most frequently performed numerically over many parameter dimensions using MCMC algorithms (Metropolis et al. 1953; Hastings 1970; Geyer 2011). A Markov chain is a random walk, where a transition from state i to state j is independent (memory-less) of how state i was populated. The fundamental theorem of Markov chains states that for a very long random walk the proportion of time (i.e., probability) the chain spends in some state j is independent of the initial state it started from. This set of limiting, long random walk, probabilities is called the stationary (or equilibrium) distribution of the Markov chain. When a Markov chain is constructed with a stationary distribution equal to the posterior, $p(\theta|y)$, the samples drawn at every step during a sufficiently long random walk will closely approximate the posterior density. Several related algorithms (e.g., Metropolis, Metropolis-Hastings, Gibbs) are known to solve this problem numerically. The combination of Bayes theorem and MCMC algorithms allows for computing models that are too difficult to estimate using traditional statistical methods.

In this work we employ the program JAGS ("Just Another Gibbs Sampler") for the analysis of Bayesian models using MCMC sampling (Plummer 2003). Specifically, we will employ the rjags package that works directly with JAGS within the R language (R Core Team 2015). Running a JAGS model refers to generating random samples from the posterior distribution of model parameters. This involves the definition of the model, likelihood, and priors, as well as the initialization, adaptation, and monitoring of the Markov chain.

4.2. *Likelihoods and Priors*

For illustrative purposes, suppose first that the experimental S-factor, S^{exp}, is free of measurement uncertainties ($\epsilon_{syst} = \epsilon_{stat} = 0$), and that it is only subject to stochastic uncertainties ($\epsilon_{stoc} \neq 0$) that follow a normal probability distribution with a standard deviation of σ_{stoc}. In that case, the likelihood can be written as

$$\mathcal{L}(S^{exp}|\theta) = \prod_{i=1}^{N} \frac{1}{\sigma_{stoc}\sqrt{2\pi}} e^{-\frac{[S_i^{exp} - S(\theta)_i]^2}{2\sigma_{stoc}^2}} \tag{12}$$

where $S(\theta)_i$ is the model S-factor (i.e., obtained from R-matrix theory), and the product runs over all data points, labeled by i. The likelihood represents a product of normal distributions, each with a mean of $S(\theta)_i$ and a standard deviation of σ_{stoc}. Symbolically, this expression can be abbreviated by

$$S_i^{exp} \sim N(S(\theta)_i, \sigma_{stoc}^2) \tag{13}$$

where N denotes a normal probability density. If the S-factor data would be subject only to experimental statistical uncertainties ($\epsilon_{stoc} = \epsilon_{syst} = 0$; $\epsilon_{stat} \neq 0$), then the likelihood is given by

$$\mathcal{L}(S^{exp}|\theta) = \prod_{i=1}^{N} \frac{1}{\sigma_{stat,i}\sqrt{2\pi}} e^{-\frac{[S_i^{exp} - S(\theta)_i]^2}{2\sigma_{stat,i}^2}} \tag{14}$$

where $\sigma_{stat,i}$ denotes the standard deviation of a normal distribution given by the statistical uncertainty of datum i. In symbolic notation, we obtain

$$S_i^{exp} \sim N(S(\theta)_i, \sigma_{stat,i}^2) \tag{15}$$

When both effects are taken simultaneously into account ($\epsilon_{stoc} \neq 0$; $\epsilon_{syst} \neq 0$), the overall likelihood is given by a nested (and cumbersome explicit) expression. In the more convenient symbolic notation, we can write

$$S_i' \sim N(S(\theta)_i, \sigma_{stoc}^2) \tag{16}$$

$$S_i^{exp} \sim N(S_i', \sigma_{stat,i}^2) \tag{17}$$

where $\sim$ stands for "distributed as" or "sampled from." The last two expressions show in an inuitive manner how the overall likelihood is constructed: first, stochastic effects, quantified by standard deviation σ_{stoc} of a normal probability density, perturb the "true" value of the S-factor at energy i, $S(\theta)_i$, to produce a value of S_i'; second, the latter value is perturbed, in turn, by the statistical experimental uncertainty, quantified by standard deviation σ_{stat} of a normal probability density, to produce the measured value S_i^{exp}.

The above demonstrates how any effect impacting the data can be implemented in a straightforward manner into a Bayesian data analysis. There is nothing special about using normal distributions in the example above, which we only chose to explain a complex problem in simple words. As will be seen below, some of the likelihood functions used in the present work are non-normal.

Each of the model parameters, contained in the vector θ, requires a prior distribution. It contains the information on the probability density of a given parameter prior to analyzing the data under consideration. For example, if our model has only one parameter, and if all we know is that the value of a parameter, θ, lies somewhere in a region from zero to θ_{max}, we can write in symbolical notation for the prior

$$\theta \sim U(0, \theta_{max}) \tag{18}$$

where U denotes a uniform probability density. Some other priors used in the present work, depending on the special circumstances, are broad normal densities truncated at zero, narrow normal densities, and log-normal densities.

5. DATA ANALYSIS

5.1. *Results with fixed input parameter values*

Although the ^{3}H(d,n)^{4}He cross section is dominated at low energies by a single resonance, any fitting procedure will face a number of interesting problems.

First, Argo et al. (1952) noted that, as is usual when fitting a resonance curve to data, an equally good fit is obtained for two possible solutions of the partial width ratio, with $\Gamma_d/\Gamma_n > 1$ and < 1, and that it is not possible to chose between them without additional information about the magnitude of the reduced widths γ_d^2 and γ_n^2. They also note, however, that the two solutions do not give widely different parameter values since the Γ_d/Γ_n ratio is close to unity.

Second, in addition to the ambiguity introduced by the ratio of partial withs, there is another complication related to their absolute magnitude. Consider the two S-factor parameterizations shown in Figure 2. The data are the same as in Figure 1. The blue curve was obtained using the best-fit values of Barker (1997) for the eigenenergy and the reduced widths ($E_0 = 0.0912$ MeV, $\gamma_d^2 = 2.93$ MeV, $\gamma_n^2 = 0.0794$ MeV); Barker's choices for the channel radii and boundary condition parameters were $a_d = 6.0$ fm, $a_n = 5.0$ fm, $B_d = -0.285$, $B_n = -0.197$. Although the data analyzed by Barker and the data evaluated in the present work (see Appendix A) are not identical, it can be seen that his best-fit curve describes the observations well. The red curve was computed by arbitrarily multiplying Barker's reduced width values by a factor of 10 ($\gamma_d^2 = 29.3$ MeV, $\gamma_n^2 = 0.794$ MeV) and slightly adjusting the eigenenergy and boundary condition parameter ($E_0 = 0.102$ MeV, $B_d = -0.267$). Notice that the red curve does not represent any best-fit result, but it's sole purpose is to demonstrate that similar S-factors can be obtained by vastly different values of the partial widths. However, the red curve represents an unphysical result if we consider additional constraints: a deuteron reduced width of $\gamma_d^2 = 29.3$ MeV, obtained with a channel radius of $a_d = 6.0$ fm, exceeds the Wigner limit (Equation 8) by a factor of 30 and is thus highly unlikely.

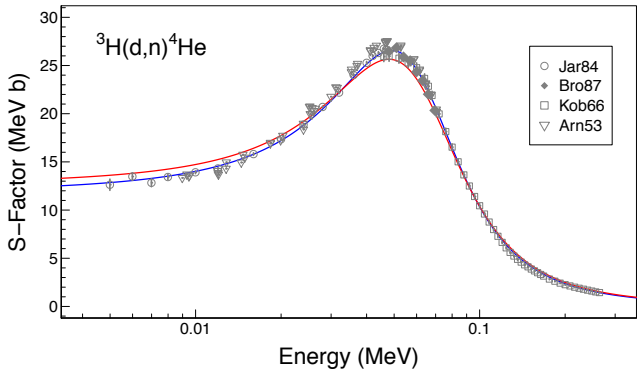

Figure 2. Astrophysical S-factors computed using the single-level, two-channel approximation (Equations 1 - 3). The data are the same as in Figure 1. The blue curve is computed with the best-fit parameter values of Barker (1997). The red curve is obtained by arbitrarily multiplying Barker's reduced widths by a factor of 10 and adjusting the eigenenergy and boundary condition parameter slightly. The red curve does not represent any best-fit result and serves for illustrative purposes only.

The latter ambiguity is caused by the structure of Equation 3. The large reduced width of the deuteron channel dominates the level shift (Equation 5) and also the factor $(E_0 + \Delta - E)$ in Equation 3. Therefore, if the reduced or partial widths for both channels are multiplied by a similar factor, the shape and magnitude of the S-factor is only slightly changed. This ambiguity in the parameter selection cannot be removed even when d

+ t elastic scattering data are simultaneously analyzed together with the recation data, as noted by Barit & Sergeev (1971).

Third, the large total width of the resonance is similar in magnitude to the resonance energy. The resonance is so broad that the experimental values of the scattering matrix element, $|S_{dn}|^2$, the cross section, σ, and the S-factor, $S_{bare}(E)$, all peak at markedly different center-of-mass energies (≈80 keV, ≈65 keV, and ≈50 keV, respectively). The differences are caused by the energy dependences of the wave number ($k^2 \sim E$) in Equation 1 and the Gamow factor ($e^{2\pi\eta}$) in Equation 2 over the width of the resonance. Furthermore, the location of the $|S_{dn}|^2$ maximum does not coincide anymore with the energy at which the factor $(E_0 + \Delta - E)$ in Equation 3 is equal to zero, because of the energy dependence of the penetration factors over the width of the resonance. Therefore, there is no unique procedure for defining an energy, E_r, "at the center of the resonance" (Lane & Thomas 1958). In other words, for the broad low-energy resonance in ^{3}H(d,n)^{4}He, we cannot chose the boundary condition parameter, $B_c = S_c(E_r)$, so that the level shift is zero at the location of the maximum of either $|S_{dn}|^2$, σ, or $S_{bare}(E)$, and at the same time expect the "center of the resonance", E_r, to equal the eigenvalue E_0 (see Section 3).[1]

For example, consider again the blue curve shown in Figure 2, which was obtained with $E_0 = 0.0912$ MeV and $B_d = S_d(E_r) = -0.285$, where the latter value corresponds to an energy of $E_r = 0.0912$ MeV. If we chose instead to set the level shift equal to zero at the location of the $|S_{dn}|^2$ maximum (i.e., $E_r = 80$ keV), the eigenenergy needs to be chosen near 140 keV to achieve a good fit to the data, while keeping all other parameters constant. In other words, the eigenenergy is not located near the $|S_{dn}|^2$ maximum anymore. Conversely, if we set the eigenenergy equal to the location of the $|S_{dn}|^2$, σ, or $S_{bare}(E)$ maximum, good fits to the data require a level shift of zero near energies of $E_r = 0.092$ MeV, 0.096 MeV, and 0.098 MeV, respectively. We will explore the impact of boundary condition parameter variations on the fit results in Section 5.3.

[1] Jarmie et al. (1984) state that they "chose B_c so that the level shifts Δ_c are zero near the peak of the S function, which results in the level energy E_λ being close to the c.m. energy at which the S function peaks." Their Table VII lists the values of $a_d = 5.0$ fm, $a_n = 3.0$ fm and $B_d = -0.27864$, $B_n = -0.557$ for the channel radii and boundary conditions, respectively. However, the latter values correspond to an energy of $E_r = 90$ keV, which, contrary to their statement, is not near the peak of the astrophysical S factor (50 keV).

5.2. *Results with fixed channel radii and boundary conditions*

We will first discuss the results of a Bayesian analysis using just three R-matrix parameters (E_0, γ_d^2, and γ_n^2). The channel radii and boundary condition parameters are kept fixed at $a_d = 6.0$ fm, $a_n = 5.0$ fm and $B_d = -0.285$, $B_n = -0.197$, i.e., the same values as used in Barker (1997). The values for the boundary conditions correspond to a level shift of zero at an energy of $E_r = 0.0912$ MeV. The electron screening potential, which will be discussed later, is set equal to zero. We are interested to find out how our parameter estimates compare to previous results.

A rigorous data analysis requires a careful distinction between statistical and systematic uncertainties, because we need to implement these effects separately in our Bayesian model. This was the main reason for considering only those data sets for which we can quantify the two contributions separately (Appendix A).

Statistical uncertainties are well understood and they usually follow a known probability distribution. When a series of independent experiments is performed, statistical uncertainties will give rise to different results in each individual measurement. The magnitude of the statistical uncertainty can be estimated from the standard deviation of the data, if the experiments are uncorrelated. All data points considered here have small statistical uncertainties (Appendix A) and, consequently, we will assume normal probability densities for the likelihood functions (Equations 12 and 14).

Systematic effects, on the other hand, do not usually signal their existence by a larger fluctuation of the data. When the experiment is repeated, the presence of systematic effects may not produce different answers. Reported systematic uncertainties are partially based on assumptions made by the experimenter, are model dependent, and follow vaguely known probability distributions (Heinrich & Lyons 2007).

The S-factor data that we will analyze have been reported with systematic uncertainties that are related to normalization factors. For example, a systematic uncertainty of, say, ±5%, implies that the systematic factor uncertainty is 1.05. The true value of the normalization factor, f, is unknown at this stage, otherwise there would be no systematic uncertainty. However, we do have one piece of information: the expectation value of the normalization factor is unity. If this would not be the case, we would have corrected the data for the systematic effect.

A useful distribution for normalization factors is the lognormal probability density, which is characterized by two quantities, the location parameter, μ, and the

spread parameter, σ. The median value of the lognormal distribution is given by $x_{med} = e^{\mu}$, while the factor uncertainty, for a coverage probability of 68%, is $f.u. = e^{\sigma}$. We will include in our Bayesian model a systematic effect as an informative, lognormal prior with a median of $x_{med} = 1.0$ or $\mu = \ln x_{med} = 0$, and a factor uncertainty given by the systematic uncertainty, i.e., in the above example, $f.u. = 1.05$ or $\sigma = \ln f.u. = \ln(1.05)$. The prior is explicitly given by

$$\pi(f_n) = \frac{1}{\ln(f.u.)_n \sqrt{2\pi} f_n} \exp\left\{ -\frac{(\ln f_n)^2}{2[\ln(f.u.)_n]^2} \right\} \quad (19)$$

where the subscript n labels the different data sets. We can write in symbolic notation

$$f_n \sim LN(0, [\ln(f.u.)_n]^2) \quad (20)$$

For more information on this choice of prior, see Iliadis et al. (2016).

Next, we need to define the priors for the R-matrix parameters. For the eigenenergy, we chose a weakly informative prior, specifically a normal distribution with a mean of zero, a standard deviation of 1.0 MeV, and restricted to positive energies only. Uniform priors are assumed for the reduced widths, with minimum and maximum values of zero and ten times the Wigner limit (Equation 8), respectively. For the prior of the stochastic uncertainty, we adopted a uniform density between zero and 5 MeVb.

Our Bayesian model contains at this stage a total of eight parameters: three R-matrix parameters (E_0, γ_d^2, γ_n^2), one normalization factor for each of the four data sets (f_1, f_2, f_3, f_4), and the stochastic uncertainty (σ_{stoc}). The full model is given in symbolic notation by

R-matrix parameters:

$$\theta \equiv (E_0, \gamma_d^2, \gamma_n^2) \quad (21)$$

Likelihoods:

$$S_i' \sim N(S(\theta)_i, \sigma_{stoc}^2) \quad (22)$$

$$S_{i,n}'' = f_n \times S_i' \quad (23)$$

$$S_{i,n}^{exp} \sim N(S_{i,n}'', \sigma_{stat,i}^2) \quad (24)$$

Priors for all parameters:

$$E_0 \sim N(0, 1.0^2) \quad (25)$$

$$(\gamma_d^2, \gamma_n^2) \sim U(0, 10 \times \gamma_{WL}^2) \quad (26)$$

$$f_n \sim LN(0, [\ln(f.u.)_n]^2)$$

$$\sigma_{stoc} \sim U(0, 5) \quad (27)$$

where the indices n and i label the data set and the data points within each set, respectively. All numerical values of energy variables are in units of MeV.

The systematic uncertainties for the data of Jarmie et al. (1984), Kobzev et al. (1966), and Arnold et al. (1953) are discussed in Appendix A and amount to 1.26%, 2.5%, and 2.0%, respectively. These correspond to factor uncertainties of $(f.u.)_1 = 1.0126$, $(f.u.)_2 = 1.025$, and $(f.u.)_3 = 1.020$, respectively. We already mentioned in Section 2 (see also Appendix A) that Brown et al. (1987) did not determine absolute cross sections, but normalized their data to the results of Jarmie et al. (1984). We will include this data set in our analysis by chosing a weakly informative prior for the factor uncertainty, i.e., $(f.u.)_4 = 100$.

The MCMC sampling will provide the posteriors for all eight parameters. We generated random samples using three independent Markov chains, each of length 75,000 (without burn-in). This ensures that the Monte Carlo fluctuations are negligible compared to the statistical and systematic uncertainties.

5.3. *Sampling With Five Parameters: E_0, γ_d^2, γ_n^2, a_d, a_n*

5.4. *Results Including Electron Screening*

6. THERMONUCLEAR REACTION RATES

xxx

7. SUMMARY AND CONCLUSIONS

xxx

We would like to thank xxx for their input and feedback. This work was supported in part by NASA under the Astrophysics Theory Program grant 14-ATP14-0007, and the U.S. DOE under contracts DE-FG02-97ER41041 (UNC) and DE-FG02-97ER41033 (TUNL).

Software: JAGS

Table 1. The ^{2}H(t,α)n Data of Jarmie et al. (1984).

$E_{c.m.}$[a] (keV)	$S \pm \Delta S_{\rm stat}$[b] (MeVb)	$E_{c.m.}$[a] (keV)	$S \pm \Delta S_{\rm stat}$[b] (MeVb)
4.992	12.63±0.58	27.996	20.70±0.09
5.990	13.48±0.39	31.998	22.19±0.11
6.990	12.83±0.40	36.001	24.02±0.11
7.990	13.43±0.27	40.004	25.28±0.14
9.989	13.92±0.14	42.005	26.00±0.12
11.989	14.32±0.10	44.007	26.30±0.14
15.990	15.81±0.13	46.009	26.74±0.13
19.992	17.35±0.09	46.809	26.64±0.14
23.994	18.87±0.08		

[a] Total uncertainty varies continuously from ±2.4 eV at $E_{c.m.}$ = 5 keV to ±6.4 eV at $E_{c.m.}$ = 47 keV.
[b] Systematic uncertainty: 1.26%.

APPENDIX

A. NUCLEAR CROSS SECTION DATA FOR ^{3}H + $D \rightarrow N + {}^4$HE

We discuss here the current status of the available data for the ^{3}H(d,n)^{4}He reaction. Several works have measured only differential cross sections at a single angle, and assumed an isotropic angular distribution to derive the total cross section. Figure 4 in Conner et al. (1952) shows that the integrated cross section points fall below the theoretical single-level dispersion curve (solid line) at deuteron bombarding energies of $\leq$ 450 keV. Therefore, at these low energies, the cross section is determined by the $3/2^+$ (s-wave) resonance in ^{3}H + d (see Section 1), and the angular distribution can be assumed to be nearly isotropic; see also Bém et al. (1997). At higher energies, higher-lying levels in ^{5}He will impact the cross section, giving rise to non-isotropies in the differential cross section. In the present work, we only take data in this low-energy range into account (corresponding to bombarding triton energies of $\leq$ 680 keV, or center-of-mass energies of $\leq$ 270 keV), which is of primary interest for ^{3}H + d thermonuclear fusion. As noted in Section 5.2, we will adopt in our analysis only those data sets for which we can separately estimate statistical and systematic uncertainties.

A.1. *The ^{2}H(t,α)n Data of Jarmie et al. (1984)*

The measurement of Jarmie et al. (1984) was performed using a triton beam incident on a windowless deuterium gas target. This technique minimizes systematic beam energy uncertainties compared to other measurements that used a gas target contained by foils. Our adopted center-of-mass energies and astrophysical S-factors are listed in Table 1. The energies ($E_{c.m.} = 5 - 47$ keV) correspond to the center of the gas target and were calculated from the laboratory energies listed in column 2 of Table V in Jarmie et al. (1984). The total (systematic plus statistical) uncertainties of the center-of-mass energies are less than 6 eV. The S-factors are taken from column 3 of their Table VI. Their statistical uncertanties amount to 0.5% − 4.6%, depending on energy (see their Table III). The systematic uncertainty is 1.26% (see their Table IV).

A.2. *The ^{3}H(d,α)n Data of Brown et al. (1987)*

The ^{3}H(d,α)n measurement of Brown et al. (1987) was performed with an apparatus similar to the one described in Jarmie et al. (1984), except that a deuteron beam ($E_d = 80 - 116$ keV) was incident on a triton gas target. However,

Table 2. The ^{3}H(d,α)n data of Brown et al. (1987).

$E_{c.m.}$ [a] (keV)	$S_{\rm rel} \pm \Delta S_{\rm stat}$ [b] (MeVb)	$E_{c.m.}$ [a] (keV)	$S_{\rm rel} \pm \Delta S_{\rm stat}$ [b] (MeVb)
47.948	26.48±0.21	59.941	24.33±0.19
50.947	26.84±0.21	62.941	23.44±0.19
53.942	25.89±0.21	65.941	22.02±0.18
56.942	25.50±0.20	69.541	20.34±0.16

[a] Total uncertainty of center-of-mass energy is ±9 eV.

[b] The values reported in Brown et al. (1987) were normalized relative to the data of Jarmie et al. (1984), listed in Table 1.

no absolute normalization was determined in Brown et al. (1987). For the purpose of reporting their data, Brown et al. (1987) determined an approximate scale by matching the cross sections in the overlapping energy region to the earlier absolute measurement of Jarmie et al. (1984). The reported astrophysical S-factors versus center-of-mass energies are listed in Table 2. Since they represent relative results only, we implemented these data into our analysis using a weakly informative prior for the normalization factor (Section 4). The statistical uncertainties amount to 0.8%.

A.3. *The ^{2}H(t,α)n Data of Kobzev et al. (1966)*

Kobzev et al. (1966) measured the ^{2}H(t,α)n cross section at 90° in the triton bombarding energy range of E_t = 115 − 1650 keV. They employed mica foils of 0.16 mg/cm^2 and 0.31 mg/cm^2 thickness as entrance windows of their deuterium gas target. Below a triton bombarding energy of 660 keV, the differential cross section is isotropic (Conner et al. 1952) and, therefore, we calculated the total cross section by multiplying the values listed in their table by 4π. Our adopted S-factors are given in Table 3. Regarding the uncertainties in the bombarding energy, Kobzev et al. (1966) state "The interaction energy of tritium and deuterium nuclei was determined with 2.5% accuracy in the range 115 − 150 keV, with 2% accuracy in the range 150 − 1200 keV....." We adopted these uncertainties (see Table 3) and assume that they refer to statistical effects. Furthermore, they state "The differential cross section was measured from 115 to 400 keV with 2% accuracy[,] in the range 400 − 800 keV with 2.5% accuracy..." Although Kobzev et al. (1966) do not provide separate estimates of statistical and systematic uncertanties, we will assume that the quoted values are of statistical nature. For the systematic uncertainty in their measurement, we assume a value of 2.5%.

A.4. *The ^{3}H(d,n)α Data of Arnold et al. (1953)*

Arnold et al. (1953) measured cross sections of the ^{3}H(d,n)α reaction between 10 keV and 120 keV deuteron bombarding energy, using thin (5 − 10 μg/cm^2) SiO entrance foils for their tritium gas target. Their results were later published in Arnold et al. (1954), and Table III in the latter paper served as the main source for their cross sections in most previous analyses; see, e.g., Angulo et al. (1999). However, Arnold et al. (1954) did not report the originally measured cross sections of Arnold et al. (1953) in their Table III. What is listed there are energies and cross sections derived from a "smoothed curve" based on the energy dependence of the Gamow factor, and these values should not be used in fitting the data. The original data are provided in Table VI of Arnold et al. (1953), and were adopted in our analysis.

We disregarded the data points at the lowest deuteron bombarding energies of 7 − 11 keV "...because failure of the counter collimating system and excess production of condensable vapor gave good reason to expect that the experimental value of the cross sections at these energies might be low." Furthermore, the listed cross section values at E_d = 24.96 keV, 24.91 keV, and 24.89 keV are certainly affected by a decimal-point error, since they are too large by one order of magnitude. Similarly, the listed cross section values at E_d = 49.62 keV and 49.60 keV are too low by one order of magnitude. Therefore, we disregarded these five data points.

Table 3. The ^{2}H(t,α)n Data of Kobzev et al. (1966).

$E_{c.m.} \pm \Delta E_{c.m.}$ [a] (keV)	$S \pm \Delta S_{\rm stat}$ [b] (MeVb)	$E_{c.m.} \pm \Delta E_{c.m.}$ [a] (keV)	$S \pm \Delta S_{\rm stat}$ [b] (MeVb)
46.0±1.2	25.93±0.52	132.0±2.6	5.23±0.10
48.0±1.2	25.96±0.52	136.0±2.7	4.89±0.10
52.0±1.3	25.76±0.52	140.0±2.8	4.60±0.09
56.0±1.4	25.28±0.51	144.0±2.9	4.32±0.09
60.0±1.5	24.77±0.50	148.0±3.0	4.11±0.08
64.0±1.3	23.66±0.47	152.0±3.0	3.88±0.08
66.0±1.3	22.85±0.46	156.0±3.1	3.69±0.07
68.0±1.4	21.89±0.44	160.0±3.2	3.50±0.07
72.0±1.4	19.98±0.40	164.0±3.3	3.32±0.08
76.0±1.5	18.14±0.36	168.0±3.4	3.15±0.08
80.0±1.6	16.53±0.33	176.0±3.5	2.84±0.07
84.0±1.7	15.01±0.30	184.0±3.7	2.62±0.07
88.0±1.8	13.65±0.27	192.0±3.8	2.42±0.06
92.0±1.8	12.50±0.25	200.0±4.0	2.26±0.06
96.0±1.9	11.41±0.23	208.0±4.2	2.13±0.05
100.0±2.0	10.45±0.21	216.0±4.3	2.00±0.05
104.0±2.1	9.59±0.19	224.0±4.5	1.89±0.05
108.0±2.2	8.76±0.18	232.0±4.6	1.79±0.04
112.0±2.2	7.98±0.16	240.0±4.8	1.69±0.04
116.0±2.3	7.28±0.15	248.2±5.0	1.60±0.04
120.0±2.4	6.65±0.13	256.2±5.1	1.51±0.04
124.0±2.5	6.08±0.12	264.3±5.3	1.44±0.04
128.0±2.6	5.61±0.11		

[a] Triton laboratory energies have a 2.5% accuracy in the range 115 − 150 keV, and a 2% accuracy in the range 150 − 1200 keV (see text).

[b] Assumed systematic uncertainty: 2.5% (see text).

Arnold et al. (1953) provide a detailed list of uncertainties in their Table VIII. Statistical uncertainties amount to 0.2% and 0.1% at deuteron bombarding energies below and above ≈ 40 keV, respectively. Our derived center-of-mass energies and S-factors are listed in Table 4. Arnold et al. (1953) quoted systematic uncertainties ("standard error") of 1.8%, 1.5%, and 1.4% at deuteron bombarding energies of 25 keV, 50 keV, and 100 keV, respectively. In our analysis, we will adopt a constant systematic uncertainty of 2.0%.

A.5. *Other Data*

The following data sets were excluded from our analysis. The data of Bretscher & French (1949) are much smaller in magnitude compared to other data, and do not show the maximum of the resonance. The S-factor data of Jarvis & Roaf (1953) display an energy dependence that contradicts all other measurements; see, for example, Figure 2 in Bosch & Hale (1992).

Table 4. The ^{3}H(d,n)α Data of Arnold et al. (1953).

$E_{c.m.}$ (keV)	$S \pm \Delta S_{\rm stat}$ [a] (MeVb)	$E_{c.m.}$ (keV)	$S \pm \Delta S_{\rm stat}$ [a] (MeVb)
8.98	13.340±0.026	31.52	22.695±0.023
9.32	13.703±0.027	35.36	24.314±0.024
9.47	13.508±0.027	35.38	24.589±0.024
9.52	13.600±0.027	37.00	24.967±0.025
11.95	14.068±0.028	37.16	25.184±0.025
11.99	13.849±0.028	41.23	26.600±0.027
12.03	13.680±0.027	41.25	26.514±0.026
12.81	14.302±0.029	43.29	27.067±0.027
12.83	14.957±0.030	42.49	26.847±0.027
14.48	14.939±0.030	46.61	27.466±0.027
14.68	15.753±0.031	46.64	27.365±0.027
14.89	15.448±0.030	46.65	27.489±0.027
18.33	16.921±0.034	47.22	27.505±0.027
18.35	16.989±0.032	47.25	27.542±0.027
19.92	17.249±0.034	52.80	26.975±0.027
20.27	17.721±0.035	52.83	27.085±0.027
23.95	18.969±0.038	58.66	25.621±0.025
23.97	18.366±0.036	58.68	25.669±0.026
25.17	20.718±0.021	61.39	24.593±0.024
25.26	20.755±0.021	61.43	24.492±0.024
25.32	19.969±0.020	64.51	23.071±0.023
25.66	19.920±0.020	64.54	23.157±0.023
25.72	20.596±0.020	67.37	22.002±0.022
26.09	20.277±0.020	67.39	21.951±0.022
26.38	20.525±0.020	70.39	20.445±0.020
29.95	21.766±0.022	70.44	20.227±0.020
31.16	22.749±0.023		

[a] Adopted systematic uncertainty: 2.0% (see text).

The cross section data of Conner et al. (1952) were obtained in two experiments, using different ion accelerators, for deuteron bombarding energies between 10 keV and 1732 keV. However, they do not report the uncertainties of the bombarding beam energy at the center of the target. Also, they do not provide any information regarding the statistical uncertainties of the cross sections at the lowest bombarding energies.

The ^{2}H(t,n)^{4}He measurement of Argo et al. (1952) employed relatively thick (1.5 mg/cm^{2}) aluminum entrance foils for their deuterium gas target. For example, tritons of 183 keV laboratory energy after passing the entrance foil would have lost 568 keV in the foil, giving rise to a beam straggling of $\approx$ 31 keV. Consequently, the uncertainties

in the effective beam energy will be significant. Argo et al. (1952) stated that the beam energy *loss* was determined "to within ±5 keV," but not enough information was provided regarding the total uncertainty of the effective beam energy. Also, Argo et al. (1952) stated that their cross section data "...have an estimated over-all accuracy of ±10%; this ±10 percent arises almost entirely from the straggling and energy correction uncertainties up to energies of about 300 keV..." However, insufficient information is provided to disentangle the contributions of statistical and systematic effects to the total uncertainty.

REFERENCES

Angulo, C., et al. 1999, Nucl. Phys. A 656, 3

Argo, H.V., Taschek, R.F., Agnew, H.M., Hemmedinger, A., & Leland, W.T. 1952, Phys. Rev. 87, 612

Arnold, W.R., Phillips, J.A., Sawyer, G.A., Stovall, Jr., E.J., & Tuck, J.L. 1953, Absolute Cross Section for the Reaction T(d,n)^{4}He from 10 to 120 keV, Tech. Rep. LA-1479, Los Alamos Scientific Laboratory, Los Alamos, NM

Arnold, W.R., Phillips, J.A., Sawyer, G.A., Stovall, Jr., E.J., & Tuck, J.L. 1954, Phys. Rev. 93, 483

Bame Jr., S.J., & Perry Jr., J.E. 1957, Phys. Rev. 107, 1616

Assenbaum, H.J., Langanke, K., & Rolfs, C. 1987, Z. Phys. A 327, 461

Barit, I.Y., & Sergeev, V.A. 1971, in: Nuclear Physics and Interaction of Particles with Matter, ed. D.V. Skobel'tsyn (Springer Science, New York)

Barker, F.C. 1997, Phys. Rev. C 56, 2646

Barker, F.C., & Woods, C.L. 1985, Austr. J. Phys. 38, 563

Bém, P., Kroha, V., Mares, J., Simecková, E., Trginová, & Vercimák, P. 1997, Few-Nucleon Sys. 22, 77

Bosch, H.S., & Hale, G.M. 1992, Nucl. Fusion 32, 611-632; Erratum: 1993, Nucl. Fusion 33, 1919

Bretscher, E., & French, A.P. 1949, Phys. Rev. 75, 1154

Brown, R.E., Jarmie, N., & Hale, G.E. 1987, Phys. Rev. C 35, 1999-2004

Brown, L.S., & Hale, G.M. 2014, Phys. Rev. C, 89, 014622

Coc, A., Petitjean, P., Uzan, J.-Ph., Vangioni, E., Descouvemont, P., Iliadis, C., & Longland, R. 2015, Phys. Rev. D 92, 123526

Conner, J.P., Bonner, T.W., & Smith, J.R. 1952, Phys. Rev. 88, 468-473

Descouvemont, P., Adahchour, A., Angulo, C., Coc, A., & Vangioni-Flam, E. 2004, At. Data Nucl. Data Tabl. 88, 203

Descouvemont, P., & Baye, D. 2010, Rep. Prog. Phys. 73, 036301

de Souza, R.S., Iliadis, C., & Coc, A. 2018, ApJ, submitted

Dover, C.B., Mahaux, C., & Weidenmüller, H.A. 1969, Nucl. Phys. A 139, 593

Duane, B.H. 1972, Rep. BNWL-1685, Battelle Pacific Northwest Laboratory, Richland, WA

Engstler, S., Krauss, A., Neldner, K., Rolfs, C., Schröder, U., & Langanke, K. 1988, Phys. Lett. B 202, 179

Geyer, C. J. 2011, in *Handbook of Markov Chain Monte Carlo*,

Gómez Iñesta, Á, Iliadis, C., & Coc, A. 2017, ApJ, 849, 134

Hale, G.M., Brown, R.E., & Jarmie, N. 1987, Phys. Rev. Lett. 59, 763

Hastings, W. K. 1970, Biometrika, 57, 97

Heinrich, J., & Lyons, L. 2007, Annu. Rev. Nucl. Part. Sci., 57, 145

Hilbe, J.M., de Souza, R.S., & Ishida, E.E.O. 2017, Bayesian Models for Astrophysical Data Using R, JAGS, Python, and Stan (Cambridge University Press)

Iliadis, C., Anderson, K.S., Coc, A., Timmes, F.X., & Starrfield, S. 2016, ApJ, 831, 107

Jarmie, N., Brown, R.E., & Hardekopf, R.A. 1984, Phys. Rev. C 29, 2031-2046; 1984, Erratum: Phys. Rev. C 33, 385

Jarvis, R.G., & Roaf, D. 1953, Proc. R. Soc. Lond. A 218, 432-438

Jaynes, E., & Bretthorst, G. 2003, Probability Theory: The Logic of Science (Cambridge University Press)

Kobzev, A.P., Salatskij, V.I., & Telezhnikov, S.A. 1966, Sov. J. Nucl. Phys. 3, 774-776

Lane, A.M., & Thomas, R.G. 1958, Rev. Mod. Phys. 30, 257

Metropolis, N., Rosenbluth, A. W., Rosenbluth, M. N., Teller, A. H., and Teller, E. 1953, J. Chem Phys., 21, 1087

Peres, A.J. 1979, J. Nucl. Mater. 50, 5569

Plummer, M. 2003, *JAGS: A program for analysis of Bayesian graphical models using Gibbs sampling*, in: Proceedings of the 3rd International Workshop on Distributed Statistical Computing (dsc 2003), Vienna, Austria, ISSN 1609-395X

R Core Team 2015, *R: A language and environment for statistical computing*, R Foundation for Statistical Computing, Vienna, Austria (https://www.R-project.org/)

Teichmann, T., & Wigner, E.P. 1952, Phys. Rev. 87, 123

Tilley, D.R., Cheves, C.M., Godwin, J.L., Hale, G.M., Hofmann, H.M., Kelley, J.H., Sheu, C.G., & Weller, H.R. 2002, Nucl. Phys. A 708, 3